Transmission of low-energy O^+ ions through ultrathin films of Ar, Kr, and Xe

N. J. Sack, M. Akbulut,* and T. E. Madey
Department of Physics and Astronomy and Laboratory for Surface Modification, Rutgers, The State University of New Jersey, Piscataway, New Jersey 08855
(Received 5 May 1994; revised manuscript received 16 September 1994)

We present a systematic study of the transmission of low-energy (<10 eV) O^+ ions through ultrathin films of Ar, Kr, and Xe. The ions are produced by electron-stimulated desorption from an oxidized W(100) crystal; they desorb from the surface in directions close to the surface normal with a peak kinetic energy of ~ 7 eV and their yield, mass/energy, and angle are measured with a digital electron-stimulated desorption ion angular distribution (ESDIAD) detector. Rare gases are condensed at ~ 25 K onto the oxidized W(100) crystal and their film thickness is determined by means of thermal-desorption spectroscopy. The O^+ ions desorbed in the presence of a rare-gas film have to pass through the film before reaching the detector. We find that 10% of O^+ can be transmitted through 1.6 atomic layers of Ar, 2.9 ML of Kr, and 4.0 ML of Xe. From the O^+ signal attenuation by films thicker than 2 ML we derive attenuation cross sections of 6.0×10^{-15} cm^2 for Ar, 2.2×10^{-15} cm^2 for Kr, and 1.5×10^{-15} cm^2 for Xe. For Xe, we observe indications that the angular distribution of the ions changes due to large-angle scattering, and for Kr (and previously for Xe) we measure a shift in the energy distribution towards lower energies; we interpret this to be due to elastic forward scattering of the oxygen ions by the Xe atoms. We attribute the attenuation of the O^+ in the films mainly to elastic backscattering; we suggest that either a high neutralization probability of O^+ in the Ar film (charge transfer) or an Ar structure different from fcc (such as blocking of O^+ by Ar) is the reason for the strong attenuation of O^+ in Ar. We find greater attenuation per monolayer for thicker films than for the first monolayer; we correlate this with the fcc structure of the rare-gas films. We discuss the energy loss of the primary electrons in the rare-gas film, the effect of the adsorption of rare gases on the electron-stimulated desorption process, and the possibility of preferential O^+ desorption through channels in the rare-gas film. We draw conclusions from our results concerning the depth of origin of secondary ions desorbed under the influence of electron, photon, or ion radiation.

I. INTRODUCTION

The interaction of electrons, photons, or ions with solids can cause the desorption of secondary particles, e.g., ions or neutrals. Based on measurements like those by Burnett *et al.*,[1] it is usually assumed that these secondaries stem from the first one or two monolayers of the solid. The depth of origin of secondary atoms and ions is an important issue for surface analytical techniques, such as secondary-ion-mass spectrometry or surface analysis by resonance ionization of sputtered atoms, which are generally accepted as giving information about the chemical composition of the topmost surface layer. It is also fundamental for investigations of desorption induced by electronic transitions, such as electron- or photon-stimulated desorption from adsorbates or compound surfaces. The question of the depth of origin of secondary ions (we will not discuss neutrals in this paper) has been addressed in several theoretical investigations[2–4] and in a few experimental papers for metals and oxides.[1,5,6] However, little work has been done on the question of the depth origin of ions from insulators, and hence the understanding of the elementary processes is rather limited.

Ions produced in a layer beneath the surface can interact with the topmost layers through various elastic or inelastic processes, such as charge transfer, as has recently been suggested,[7] and elastic scattering.[8,9] These processes can change the energy, trajectory, and charge state of the ions. However, the interaction of these low-energy ions (<10 eV) with monolayers or multilayers of various materials is not well understood. We are currently investigating the transmission of 1-10 eV ions through films of rare gases and of molecular adsorbates, ranging from fractional monolayer to several multilayers in thickness. In the experiments described here, the ions are produced by electron-stimulated desorption (ESD) from an oxidized tungsten(100) crystal; this can be viewed as a "small ion beam accelerator" with a peak energy of ~ 7 eV. The ions then have to pass through an ultrathin film condensed on the crystal (Fig. 1) before being detected by a position, mass, and energy resolving ESDIAD (electron-stimulated desorption ion angular distribution) detector.[10]

In this paper, we present the total transmission yield of oxygen ions through ultrathin films of argon, krypton, and xenon as a function of film thickness. Furthermore, we analyze the angular and the energy distribution of the transmitted ions. We have chosen rare gases as overlayers because they represent the simplest physisorption systems; we expect that there is little electronic coupling between the adsorbate and the substrate. Furthermore, the oxide may be considered as a relatively rigid structure with binding energies between the oxygen and the tungsten much higher than those between energies be-

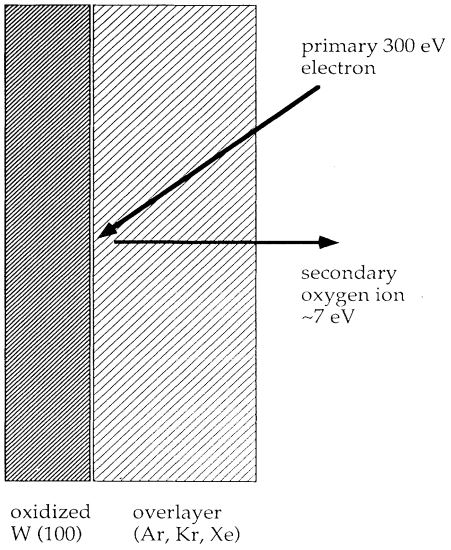

FIG. 1. Schematic of experimental approach.

tween the oxygen and the tungsten much higher than those between rare gas and substrate. Hence there is no chemically driven intermixing between the substrate and the overlayer. The following paper by Klein, Urbassek, and Vicanek[11] presents results from a molecular-dynamics (MD) simulation on the transmission of low-energy oxygen ions through thin rare-gas films. We compare their results to our experimental data.

II. EXPERIMENTAL SETUP

The experiments are carried out in an ultrahigh vacuum chamber (base pressure is $<10^{-8}$ Pa) that is equipped with instruments for various surface analytical techniques, such as thermal desorption spectroscopy (TDS), low-energy electron diffraction (LEED), Auger electron spectroscopy (AES), and ESDIAD.

The sample, a W(100) crystal, is mounted on an assembly that is coupled to a closed-cycle helium refrigerator, which enables us to cool the sample to 20 K. The sample can be heated by radiative heating and electron-beam heating with a tungsten filament mounted behind the sample. The W crystal is cleaned by heating and sputtering. It is oxidized at 860 K in an O_2 atmosphere (5×10^{-6} Pa) for 10 min, a procedure that produces a thin oxide film on the crystal.[10,12,13]

The oxide surface prepared in this way exhibits a (1×3) LEED structure. The surface is essentially clean as determined by means of AES with a small trace of carbon as an impurity, and we assume the stoichiometry to be about WO_{2-3}, based on the results of earlier investigations.[12,13]

The overlayer gases are dosed via a leak valve through a directed doser equipped with a capillary array plate onto the cold crystal. This procedure allows precise dosing from fractional monolayer to multilayer coverages of the gases. We measure the exposure in units of Langmuir ($1\ \mathrm{L}=1.33\times10^{-4}$ Pa s); however, since our ion gauge is not calibrated the absolute exposure value may not be accurate. The purity of the gases is checked in the gas phase by mass spectrometry and after adsorption by AES. An upper limit of the contamination is estimated to 0.5%.

Electron bombardment (300 eV) of the clean oxidized W(100) surface results in the desorption of oxygen ions that can be detected with our digital ESDIAD detector. This consists of a set of four high-transparency planar grids of which all except the second are grounded, a stack of five microchannel plates, and a resistive anode encoder that allows direct digital acquisition of two-dimensional data. The mass/energy resolution is achieved by pulsing the primary electron beam, which provides a start pulse coincident with desorption from the target, and gating the retarding potential grid G_2 which allows ions of flight time t_f to strike the detector [time-of-flight (TOF) method]. Since most ions desorb with kinetic energies of a similar order of magnitude (i.e., a few eV), ions arriving at different times at G_2 can be identified as having different masses, and within one mass, as having different kinetic energy. Typical electron pulse lengths are 0.1 μs with average electron currents of <1 nA, and total electron fluences are $\sim2\times10^{13}$ cm^{-2} (beam area: ~1 mm^2); the flight time for O^+ is about 3 μs. Angle-integrated ion count rates are of the order of 2×10^3 s^{-1}. The polar angle of detection (under field free conditions around the crystal) ranges from 0° to 22° (0° is normal to the surface).

The application of a positive bias voltage to the substrate compresses the angular distribution of the desorbing ions so that even ions that desorb with an angle larger than 22° can be detected. The larger the initial polar angle of desorption and the higher the initial kinetic energy of the desorbing ion, the higher the sample bias that is necessary to attract the ion into the detector. For instance, ion trajectory calculations show that a sample bias of +100 V enables the detection of a positive ion with a kinetic energy of less than 7 eV if it leaves the surface with an angle of desorption (polar angle) of less than 70° relative to the surface. Unfortunately, the application of a sample bias makes the quantitative determination of the angular distribution of the desorbing ions more difficult, because it distorts the ions trajectories and causes electric-field inhomogeneities between the sample and the detector; it furthermore does not allow determination of the kinetic-energy distribution of the ions with the ESDIAD/TOF detector. Hence a substrate bias of +100 V is applied in cases where we want to determine a quantity close to the total O^+ desorption yield, and of 0 V when we want to determine the angular or energy distribution.

In summary, the ESDIAD detector allows mass, energy, and angle-resolved measurements of the O^+-ion yield.

We can detect ESD ions also with the mass spectrometer with its ionizer turned off. This enables us to confirm the total yield of ions and their mass and angular distribution. The disadvantage of this method is that it requires higher electron current fluences due to a lower response function of the mass spectrometer and a smaller solid angle of detection, compared to the ESDIAD detector.

III. RESULTS

A. Oxygen-ion emission from the oxidized W(100) crystal

Electron-stimulated desorption from the oxidized W(100) crystal leads to a very reproducible normal emission of O^+ (maximum variation of $\sim 10\%$ in yield and angular distribution for different oxidations).[10] The O^+ beam has an angular full width at half maximum (FWHM) of $\sim 14°$. The desorption yield and angular distribution do not change significantly ($< 10\%$) upon bombardment with electron fluences up to 1×10^{16} cm^{-2}, which is much larger than any fluence used in the described experiments. The pattern does not change beyond experimental uncertainty as a function of temperature between 20 and 50 K. We can, therefore, conclude that the oxide layer is very stable and yields reproducible emission of O^+ upon electron bombardment. We confirm the identification of the ions as O^+ with the mass spectrometer. As can be seen in Fig. 2, only O^+ is present in the desorption spectrum. We have also confirmed the angular distribution with the mass spectrometer, measuring the yield as a function of the azimuth angle of the sample; the FWHM is $15\pm2°$. The energy distribution of the ions can be measured with the ESDIAD detector by applying a retarding voltage on grid G_2 and is discussed in detail later.

The emission of O^+ from this surface is in agreement with previous investigations:[14–16] Madey, Czyzewski, and Yates found strong normal O^+ emission from W(100) exposed to O_2 at 100 K and annealed at 950 K.[15] Prigge, Niehus, and Bauer also reported strong normal emission of O^+ for annealing temperatures of around 950 K of an O_2 predosed W(100) surface.[16] They furthermore report a mean energy of the O^+ of about 7 eV.

The ESD process of O^+ from oxidized tungsten can be understood by means of a model that has been developed for highly ionic maximal valency oxide surfaces.[17,18] The incoming electron can ionize W core levels (W 4*f*, W 5*p*, etc.), which can be filled through an interatomic Auger mechanism. Subsequent charge transfer from a neighboring O ion will return the W to its original (positive) charge state and can result in the formation of a positive O ion. The repulsive nature of this configuration may lead to the ejection of O^+ from the surface. Since the O^+ ions are found to desorb normal to the surface we assume that the desorbing O^+ ions come from binding sites on top of W atoms.

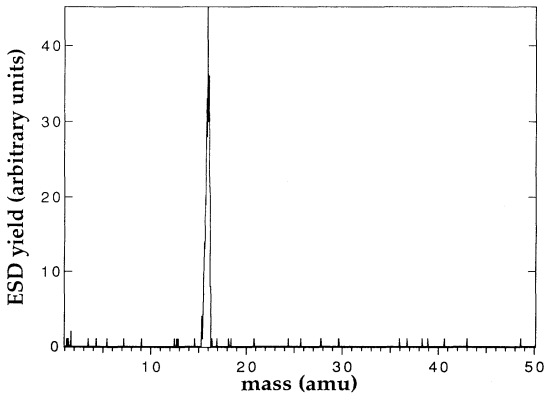

FIG. 2. Mass spectrum measured with the mass spectrometer in the ion detection mode of ESD from oxidized W(100).

B. TDS of rare gases on the oxidized W(100) crystal

We determine the rare-gas coverage by TDS. Monolayer identification is possible if the desorption peaks from the first monolayer and subsequent layers occur at different temperatures. Then the relation between coverage and exposure can be measured and calibrated.

As an example, we show in Fig. 3 uncorrected (nonbackground-subtracted) TDS spectra for Kr adsorbed on the oxidized W(100) crystals. Three peaks are separated; we identify the high-temperature peak, α_1, as the monolayer peak. The monolayer peak shifts down in temperature with increasing exposure and saturates at an exposure of 0.03–0.04 L, and the second layer peak, α_2, starts growing after completion of the monolayer peak. Finally, the multilayer peak (peak at the lowest desorption temperature, γ) starts to grow and continues to increase with increasing exposure. The integrated intensity (proportional to the coverage) after background subtraction

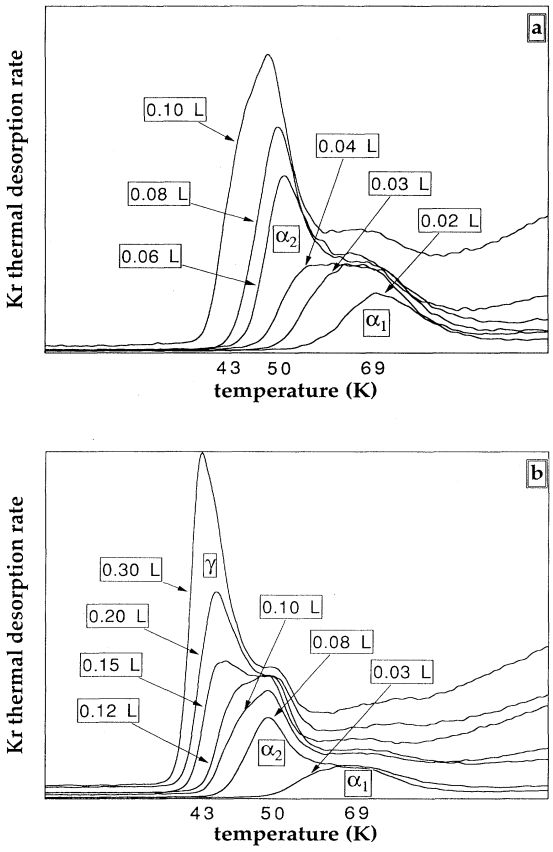

FIG. 3. TDS (thermal desorption spectra) of krypton on oxidized W(100), (a) low exposure range, (b) high exposure range. Note that the temperature scale is not linear. 1 ML$\approx$0.04 L; 2 ML$\approx$0.08 L. See text for peak identification.

increases linearly with exposure. Opila and Gomer[19] investigated the thermal desorption of Kr from oxygen predosed W(110) and came to conclusions about the peak identification similar to our interpretation. Similar investigations have been performed for Ar and Xe.[10] Details of the TDS measurements and their interpretation are discussed in detail in a separate paper.[20]

Experimental studies of the growth morphology of condensed rare-gas films on transition-metal surfaces indicate a layerwise growth.[21] Our data are consistent with the growth of rare gases in a layer-by-layer fashion also on our oxidized W(100) surface. This is supported by the separation of the first, second, and multilayer peaks and the decrease in peak temperature with increasing layer. Also, the areas of the first and second layer peaks are similar for Kr and Xe, which indicates that the surface atom densities of the first and the second layer are the same. For Ar, the TDS data suggest that the atom density of the first layer may be slightly lower than that of the second layer. Detailed bilayer experiments involving two rare gases support a layer growth mode, and are discussed elsewhere.[20]

C. Oxygen-ion desorption through thin films of Ar, Kr, and Xe

The total, angle-integrated O^+ yields as a function of overlayer coverage of Ar, Kr, and Xe obtained with a bias voltage of +100 V on the crystal are depicted in Figs. 4-6. All data have been obtained at a substrate temperature of 25 K with the ESDIAD detector, for a primary electron energy of 300 eV and a total electron fluence of $\sim 2\times 10^{13}$ cm^{-2}. The various data points represent different measurements on the same film, as well as measurements on different films, some of which were annealed close to the desorption temperature prior to measurement. The measurements are reproducible, not only on the same film, but also on different films, and annealing does not cause any systematic changes. In subsequent measurements of the O^+ yield on the same rare-gas film, we do not observe any dependence of the yield on the electron fluence, which indicates that radiation damage does not affect our results. We have obtained similar attenuation curves using the mass spectrometer as the detector instead of the ESDIAD detector which confirms the presented results.

It can be seen that some O^+ ions survive transmission of more than one monolayer of rare gas: The yield decreases to 67% after 1 ML of Ar, 63% after 1 ML of Kr, and to 67% after completion of 1 ML of Xe. The signal decreases to 10% of the value from the clean oxidized surface after 1.6 ML of Ar, 2.9 ML of Kr, or 4.0 ML of Xe. As can be seen in Figs. 4(b), 5(b), and 6(b), the yields decrease exponentially in the high coverage regime.

For Kr and Xe, we have investigated in more detail the angular and energy distribution of the O^+ ions after passage through the rare-gas film. The FWHM of the angular distribution of the O^+ desorption beam, measured with a sample bias of 0 V, does not change beyond experimental uncertainty (±1°) as a function of overlayer coverage for Kr and Xe up to 3 ML, as shown in Fig. 7. Due

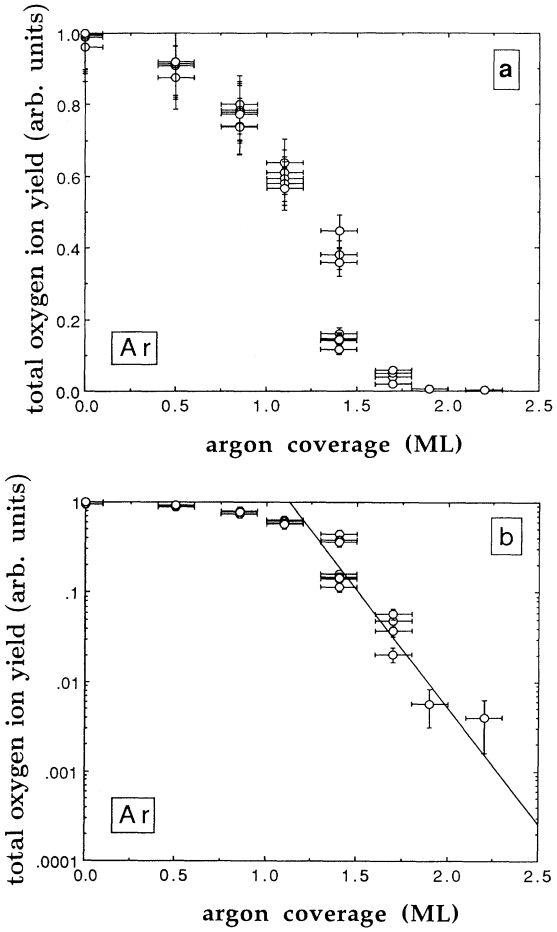

FIG. 4. (a) Total O^+ yield as a function of argon coverage (sample bias is +100 V). Lines, see text. (b) Same data as semilogarithmic plot; the line is the exponential curve fit (see text).

to limited signal-to-noise ratio, no measurements were made at higher coverage.

As mentioned in the experimental section, a difference of the measured attenuation cross section derived from measurements made with zero-volt sample bias as compared with +100-V sample bias is indicative of large-angle scattering, because ions scattered in the film by large angles cannot reach the detector for 0-V substrate bias. The application of a substrate bias of +100 V causes most of the ions to be deflected into the detector (Sec. II) and the measured yield is higher. We have observed such a deviation for Xe, shown in Fig. 8. The signal decreases faster for those measurements performed with a sample bias of 0 V than for those done with +100 V. Furthermore, for a sample bias of 0 V we depict the yields for two different O^+ energies, one around 6 eV, the other around 8 eV, each with an energy width of about 1 eV. Although the data are noisy, the attenuation seems slightly stronger for the faster oxygen ions, which could indicate that some fast ions have scattered elastically and become slow ions. It is worth noting that the difference in attenuation occurs for film thicknesses above 2 ML; we

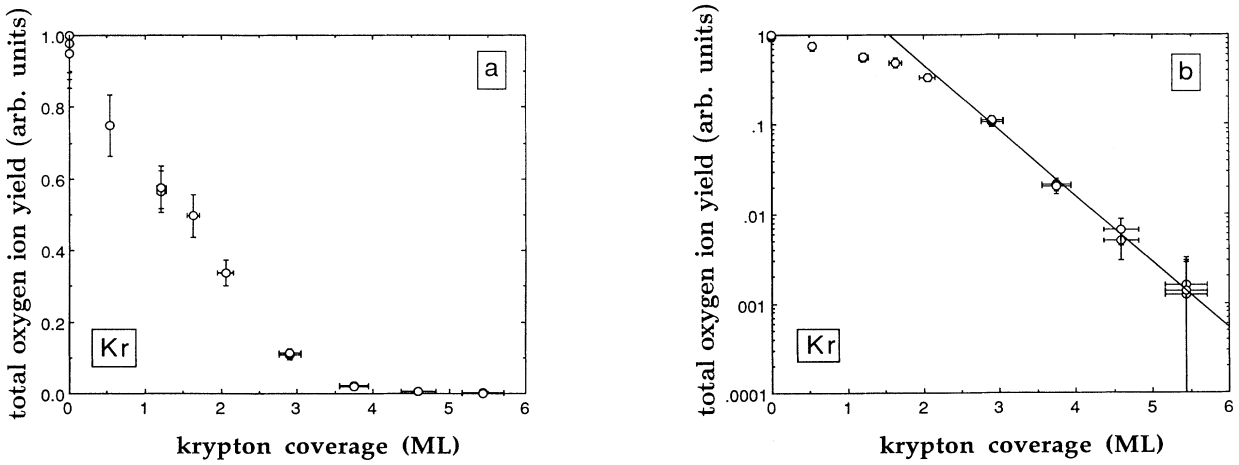

FIG. 5. (a) Total O^+ yield as a function of krypton coverage (sample bias is +100 V). Lines, see text. (b) Same data as semilogarithmic plot; the line is the exponential curve fit (see text).

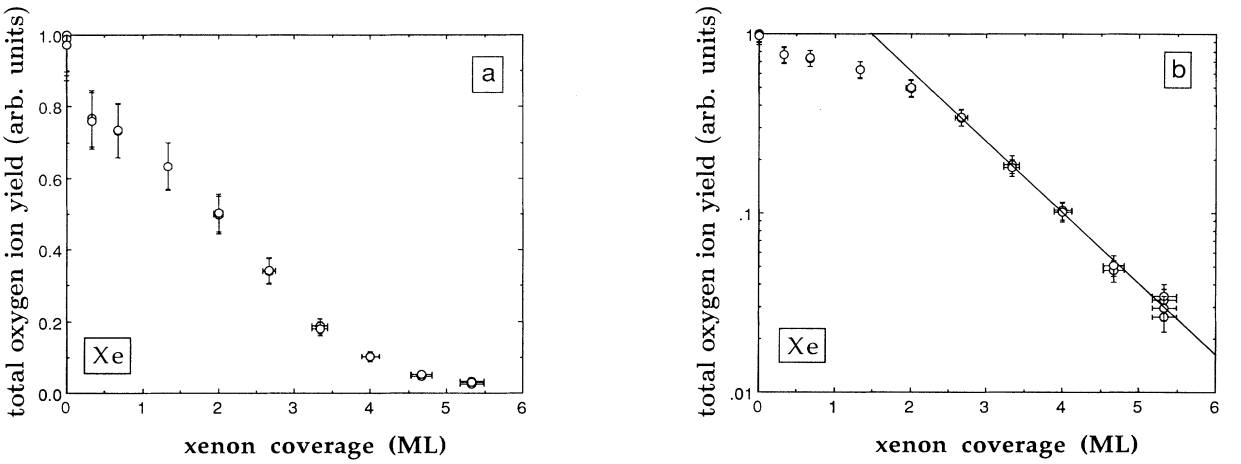

FIG. 6. (a) Total O^+ yield as a function of xenon coverage (sample bias is +100 V). Lines, see text. (b) Same data as semilogarithmic plot; the line is the exponential curve fit (see text).

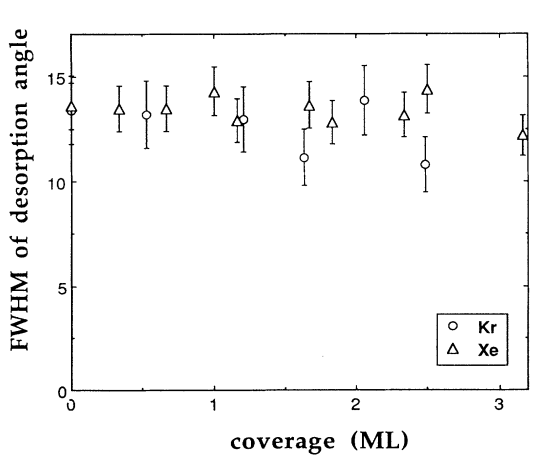

FIG. 7. FWHM (in degrees) of the O^+ beam as a function of overlayer thickness for Kr and Xe.

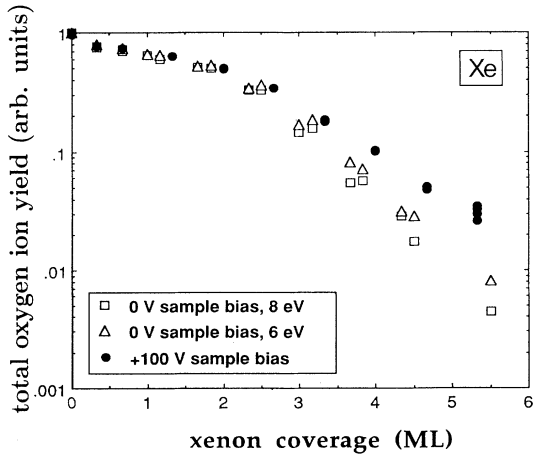

FIG. 8. Total O^+ yield as a function of xenon coverage for two different sample bias conditions and two ion energies.

discuss this later. For Kr, the scatter in the data is too large to allow similar conclusions.

Finally, we analyze the energy distribution of the O^+ ions, measured with a retarding field method, after passing through the overlayer of Kr or Xe, and compare them to the distribution of O^+ from the clean surface [Figs. 9(a) and 9(b) for Kr; see Sack, Akbulut, and Madey[22] for Xe]. No measurable change occurs for a Kr overlayer measured with a sample bias of 0 V. However, upon applying a sample bias of +100 V (which attracts into the detector ions that are scattered by large angles), we observe that the mean energy decreases for both Kr and Xe layers [Fig. 9(b); Fig. 2 in Sack, Akbulut, and Madey[22]]. This indicates that only those ions that are scattered by large angles (detected only in the +100-V case) lose a significant amount of energy on their passage through the film, not those measured for 0-V bias. It is very important, however, that the change in the kinetic-energy distribution is only seem for films thicker than 2 ML. This means that for thinner films, we do not have experimental indication that ions which can desorb from the surface as ions have lost a significant amount of their kinetic energy. Again, the coverage over which a determination of the kinetic energy is possible is limited to the energy range depicted due to low signal-to-noise ratio at higher coverages.

Note that the planar design of the ESDIAD detector allows only detection of the kinetic-energy component perpendicular to the detector (and to the surface) and neglects the parallel component. For 0-V sample bias and small desorption angle this effect is negligible. For 100-V sample bias, it leads to seemingly lower measured energy values for ions which desorb with large polar angles. In order to evaluate the contribution of this effect to the low-energy peak in the O^+ energy distribution [Fig. 9(b)] we have performed model calculations in which we assume various angular distributions of the ions and estimate their energy as measured by the planar detector. Although there is a low-energy shoulder in the simulated energy spectra, we have not seen a peak in the energy distribution around 3.5 eV as seen in the experimental data. We conclude that although the detection geometry leads to an artifact seen at lower energies, the peak shown in Fig. 9(b) [and similar data for Xe (Ref. 22)] relates to particles that have lost energy.

Since Ar leads to such strong attenuation of O^+, similar energy and angle-resolved measurements were not possible for Ar for films thicker than 2 ML due to a low signal-to-noise ratio.

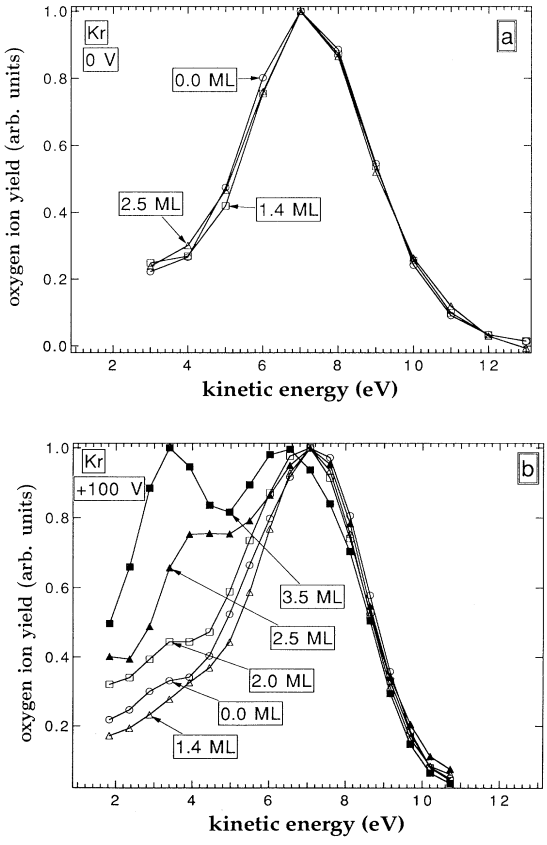

FIG. 9. Energy distribution of the O^+ ion after passage through a Kr film of various coverage (in monolayers), measured by the retarding-field method. (a) 0-V sample bias and (b) +100-V sample bias. All yields are normalized to 1 at their maximum. See text for explanation.

IV. DISCUSSION

A. Electron transport through the rare-gas film and the ESD process

First, we evaluate the effect of energy loss of the primary electrons in the rare gas on the observed O^+ attenuation. It has been reported that gas phase ionization cross sections for rare gases by 300-eV electrons are 2.2×10^{-16} cm^2 for Ar, 2.8×10^{-16} cm^2 for Kr, and 4×10^{-16} cm^2 for Xe.[23] This means that the electrons have not lost a major fraction of their kinetic energy on their passage through a rare-gas film of thickness up to 6 ML, assuming an average energy loss per ionization (W value) of about 25 eV. Furthermore, the electron-stimulated desorption of O^+ does not depend strongly on the primary electron energy around 300 eV.[24] Hence we assume that the effect of the electron-beam attenuation in the rare-gas overlayer on the O^+ desorption process can be neglected. Note that the electron scattering probability from the oxidized W(100) surface could be modified by the rare-gas overlayer, so that the flux of electrons changes as a function of film thickness. However, we expect this effect to be too small to explain the attenuation observed here.

The electron fluence used in the described measurements is very low, 2×10^{13} cm^{-2}. This (and the fact that we have not observed any dependence of the measured parameters on the electron fluence) ensures that the probability that an O^+ ion desorbs through an area in the rare-gas film that is perturbed by the passage of a previous electron is very low. However, a more important issue is whether the same electron that causes the ESD of an oxygen ion has also disturbed the rare-gas film, e.g., through excitation or ionization of a rare-gas atom. The

excitation of the rare-gas atom could lead to the formation of metastables or dimers in the rare-gas film, or to the desorption of a rare-gas atom, which could affect the interaction of the oxygen ion with the rare-gas film. Although the ionization cross sections mentioned above seem large enough for this process to occur, one has to remember that not every ionization will lead to dimer formation or rare-gas desorption, because excitations are strongly quenched when the rare-gas is adsorbed on a surface. In fact, it has been reported that the total Xe desorption cross section from an oxide surface is only 3×10^{-19} cm^2.[25,26] Furthermore, the large mass difference between oxygen and the rare gases allows rare-gas atoms that have been excited by the primary electron beam to move only a small distance during the time it takes for the oxygen ion to travel through the rare-gas film: If we assume an energy of 0.5 eV for xenon atoms, then they will move <1 Å in the time it takes for O^+ to travel through a xenon film 2 ML thick. Since the xenon atoms interact with each other they will most probably be scattered back and forth, so that the idea of there being a window in the rare-gas film through which O^+ can escape without significant interaction with the rare-gas atoms is unlikely. Although we do not exclude the possibility of O^+ desorption through a disturbed film, it seems improbable that this affects the measured parameters significantly.

Another source of disturbance of the rare gas could be the ionization and/or excitation by secondary electrons emitted from the oxide under impact or the primary electrons. In order to evaluate this effect we have measured the secondary electron yield and energy distribution from the clean oxidized W(100) surface. In Fig. 10, we show the number of secondary electrons leaving the surface per primary electron as a function of the sample bias. The secondary electron yield is 1.1 (for a sample bias of 0 V), and only about 25% of the secondary electrons have energies larger than 25 eV, which is of the order of the energy required for a rare-gas ionization (W value). Hence we conclude that secondary electrons from the oxide do not affect the rare-gas film significantly and are, therefore, not a problem in our measurements.

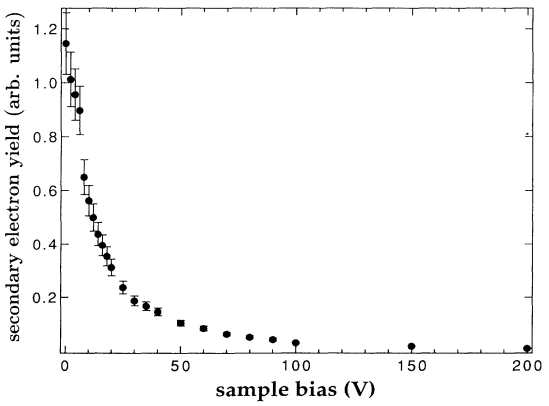

FIG. 10. Number of secondary electrons emitted from clean oxidized W(100) surface as a function of (positive) sample bias.

Based on ESD measurements from the uncovered oxidized crystal ($d=0$) we derive an oxygen-ion desorption yield on the order of 10^{-6} ions/electron, in agreement with earlier work.[15] It is possible that the adsorption of an overlayer on the oxidized W surface affects the ESD process such that excited states are quenched due to W-RG or O-RG interactions (RG=rare gas), which would lead to changes in the yield of O^+, as has been suggested previously.[25,26] Whereas this may be a problem for low rare-gas coverages, we assume that the oxygen-ion desorption yield does not change strongly upon adsorption of the rare gas for coverages higher than 1 ML, since the rare-gas atoms interact only weakly with the surface.

B. Rare-gas film structure and O^+ transport through the film

If the rare-gas films were not homogeneous in thickness but had small holes due to vacancies or defects (e.g., grain boundaries) extending through the film, one could speculate that the oxygen ions observed in the presence of a rare-gas film are those desorbing through holes. Therefore, the measured attenuation length might not be correlated to physical processes occurring during the transport of the O^+ through the film, but to the closing of holes with increasing exposure. However, there is strong experimental evidence that rare gases grow in a layer-by-layer fashion.[20,21] Also, in some experiments with various coverages of Ar, Kr, or Xe we anneal the films at a temperature close to the thermal-desorption temperature and compare the O^+ yield to that derived from the unannealed films. No difference in yield is observed ($<5\%$). Since the binding energy of the rare-gas layers decreases with increasing layer number (see Fig. 3, also Ref. 20), we expect that if islands and holes were present in the freshly deposited films, they would be reduced upon annealing and thereby decrease the O^+ yield. Hence we do not think that preferential O^+ desorption through holes in the rare-gas film is a significant factor in our experimental results. This is also supported by the molecular-dynamics simulations by Klein, Urbassek, and Vicanek:[11] As is discussed below, they model the elastic scattering of O^+ in the rare-gas films assuming a perfect fcc structure without holes due to defects, and they find excellent agreement with the experimental data, suggesting that desorption through holes does not play a significant role in the experiments.

Since we observe O^+ desorption with an angular distribution centered about the surface normal, it is highly unlikely that the O^+ desorb from edge sites, because this often leads to desorption in off-normal beams.[27,28] This is important because O^+ desorption from edge sites which might not be covered by the first or second rare-gas layer could be seen as a reason for the low attenuation in the first two monolayers.

But why is it that oxygen ions can penetrate rare-gas films several monolayers thick? To answer we recall that bulk rare-gas solids are known to be fcc structures, as shown in Fig. 11; the layer structure can be described as *A-B-C*. We have drawn the lattice to represent Kr, and the radius of the atoms to be the distance of closest ap-

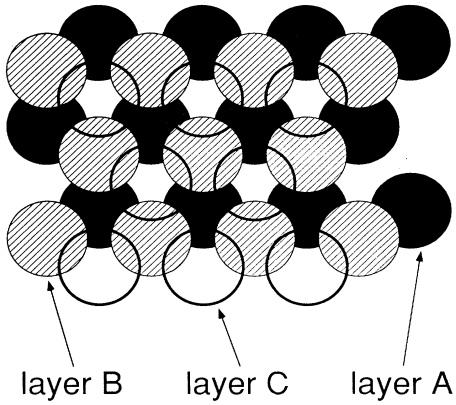

FIG. 11. Rare-gas fcc (111) structure. The atomic radii represent the 7-eV turning point in the O^+-Kr interaction, the atomic spacing represents the Kr lattice. See text.

proach of O^+ to Kr. The latter value has been derived by Klein, Urbassek, and Vicanek[11] from the potential-energy surface published by Guest *et al.*:[29] They estimate the distance for a potential of 7 eV (our O^+ peak kinetic energy) for KrO^+, $R(V=7\text{ eV})$ to be about 1.55 Å. Therefore, the circles represent a geometrical area that cannot be penetrated by the O^+ ion. Rather than looking dense for the oxygen ions, the rare-gas film has channels through which the oxygen ions may move; note that the ionic radius of O^+ is only 0.22 Å.[30] It can be seen that even after completion of the second layer, there are still channels normal to the surface through which the O^+ ion could escape without much interaction with the rare-gas atoms. Only after the completion of the third layer are these channels closed, and the oxygen ions must change their trajectory in order to penetrate the film. Hence we suggest that some form of channeling allows the O^+ ions to transmit the rare-gas film without significant energy loss or change of trajectory for coverages up to 2 ML, as has been observed in our measurements; beyond 2 ML, channeling perpendicular to the surface is hindered due to the fcc growth of the rare-gas solid, and some of the ions lose kinetic energy on their passage through the film or change their trajectory [see Fig. 9(b), Fig. 8]. We furthermore suggest that this could be the reason why, for all three rare gases, the attenuation is less for the first two monolayers than for the multilayer range. (Note that if the rare-gas films grew in the hcp structure on the oxidized W(100) surface,[31] there would be channels for film thicknesses even beyond 2 ML.)

In fact, we can compare the channel size with the transmission yield of O^+ through one or two monolayers of rare gas. We can estimate the percentage of 1 ML of RG which is blocked for O^+. For this we determine from the potential-energy surfaces for O^+-RG (Ref. 11) the internuclear distance R at which the potential between O^+ and the rare gas has the value of the peak kinetic energy of the oxygen ions, 7 eV. Then we assume that per rare-gas atom, the area blocked for the O^+ ion corresponds to a circle with radius $R(V=7\text{ eV})$. Comparing the blocked area to the unit cell of the rare-gas atom in the solid, we can derive the percentage of the rare-gas area that is blocked for O^+. For all rare gases this percentage is of order 50%; the percentage of O^+ that is transmitted through the first monolayer of rare gas is of order 60%. We suggest that there exists a correlation between the channel size and the transmission yield.

Note that we observe changes in the energy distribution of O^+ as a function of film thickness [Fig. 9(b)]. This implies that the collision parameters, such as energy and angle, for elastic scattering events may be different in the first monolayer from those in a higher layer. If the elastic scattering cross sections are a strong function of energy and angle, then this could be another reason for the change in attenuation per monolayer with increasing film thickness.

The differences in attenuation of the O^+ yield in the fractional monolayer range [see Figs. 4(a), 5(a), and 6(a)] may be a consequence of the growth mode of the rare-gas film. It has been reported for Ar adsorbed on MgO(100) that, for fractional monolayer coverages, the rare-gas atoms adsorb on preferential substrate sites (commensurate overlayer structure), whereas upon completion of 1 ML the rare-gas film ignores the substrate structure and grows in its favored fashion, a fcc (111) structure (incommensurate growth).[32] This could lead in the fractional monolayer regime to an attenuation that varies as a function of thickness: For instance, if the first atoms are adsorbed on sites where they are very effective in attenuating the O^+ ions, then the O^+ yield should decrease strongly at very low coverages, and then less as one monolayer is completed, since the rare-gas atoms are pushed into an fcc structure.

For thicker films (>2 ML for Kr and Xe; >1.5 ML for Ar) we describe the transport of the oxygen ions through the rare-gas film by a transport model that is based on Poisson statistics of the collisions:

$$\frac{\partial\Phi}{\partial d} = -N_{\mathrm{RG}}\sigma_{\mathrm{exp}}\Phi \tag{1}$$

with Φ being the total O^+ flux reaching the detector, N_{RG} is the rare-gas number density (atoms/unit volume), σ_{exp} is the attenuation constant, and d is the rare-gas film thickness. We can then write

$$\Phi=\Phi_0\exp(-N_{\mathrm{RG}}\sigma_{\mathrm{exp}}d) \tag{2}$$

with Φ_{O} being the total O^+ flux desorbing from clean oxidized W(100). If

$$d \ll 1/N_{\mathrm{RG}}\sigma_{\mathrm{exp}} \tag{3}$$

then Eq. (2) can be approximated by

$$\Phi=\Phi_0(1-N_{\mathrm{RG}}\sigma_{\mathrm{exp}}d)\ . \tag{4}$$

We have to be aware of the fact that this model is only valid if our system can be described by Poisson statistics. The fact that we observe layerwise growth of the rare-gas films violates Poisson statistics and can lead to deviations from the expected exponential attenuation within each monolayer. Also, if for fractional monolayer thicknesses the rare gases adsorb on preferential sites, this could lead to further deviations. Finally, it is important to

remember that this model is strictly valid only for binary collisions, not for multiple collisions.

From Figs. 4(b), 5(b), and 6(b) we observe exponential attenuation for films thicker than about 2 ML (1.3 ML for Ar). For this thickness range we derive the attenuation constant using the expression

$$\sigma_{\text{exp}} = -\frac{1}{N_{\text{RG}}} \frac{\partial(\ln\Phi)}{\partial d} , \tag{5}$$

which is obtained from Eq. (2). The attenuation constants can be derived from the slopes of the lines in Figs. 4(b), 5(b), and 6(b), using number densities of 2.66×10^{22} cm^{-3} for Ar, 2.17×10^{22} cm^{-3} for Kr, and 1.64×10^{22} cm^{-3} for Xe (bulk values) as follows:[33] $6.0\pm0.8\times10^{-15}$ cm^2 for Ar, $2.2\pm0.3\times10^{-15}$ cm^2 for Kr, and $1.5\pm0.2\times10^{-15}$ cm^2 for Xe.

Since the attenuation in the thick-film regime is exponential, it seems reasonable to identify the attenuation constants σ_{exp} in this regime as experimental attenuation cross sections. Note, however, that they are derived at film thicknesses at which the energy distribution of the O^+ ion is slightly different from that of O^+ from the clean oxidized W(100) surface. We will use these values of the cross section in the following discussion.

The application of a bias voltage of +100 V to the sample attracts not only those ions into the detector that desorb with a polar angle smaller than 22°, but also ions that desorb with a polar angle considerably larger than 22°. Hence these experimental attenuation cross sections can be influenced by any process in the rare-gas film or close to the surface that prevents the O^+ ion from reaching the detector.

C. Attenuation model

Now we address the reasons for the attenuation of O^+ in the rare-gas films. We suggest here a model in which the attenuation of the O^+ signal is caused by the interaction of the oxygen ions with the rare-gas film, rather than by the filling of holes and defects in the film,

$$\sigma_{\text{exp}} \equiv \sigma_{\text{tot}} \tag{6}$$

with σ_{tot} being the total O^+ attenuation cross section in the rare-gas film.

We furthermore suggest that the main scattering processes that lead to the attenuation of O^+ are elastic scattering (es) with scattering angles large enough to inhibit the escape of the scattered O^+ from the surface, and charge transfer (ct):

$$\sigma_{\text{tot}} = \sigma_{\text{es}} + \sigma_{\text{ct}} . \tag{7}$$

Elastic scattering cross sections are known to be large for small collision energies,[34] and charge transfer between ion and atom could also be important, dependent on the specific reaction.[34] We will not consider other inelastic processes, such as excitation of the overlayer species by O^+, because they are assumed to have rather low cross sections at the collision energies discussed here.[9,34]

In the following, we discuss the various contributions of elastic scattering and charge transfer to the attenuation.

1. Elastic scattering

Elastic scattering leads to changes in the trajectory and the kinetic energy of an oxygen ion. To simplify the following discussion we assume that the O^+ desorb normal to the surface (the FWHM of the angular distribution is 14° centered on the normal). In the case of scattering by an angle of 90° or more we expect the ion not to be able to desorb from the surface; the ion neutralizes and finally either desorbs as a neutral particle or it may become trapped in the rare-gas film. If the ion is forward scattered (by an angle $<90°$), it may desorb from the surface.

The fact that the FWHM of the angular distribution of O^+ (measured for a sample bias of 0 V) does not change within the experimental uncertainty as a function of coverage up to 2−3 ML (Fig. 7) indicates that scattering of surviving ions is rare in this coverage regime; also the data in Fig. 8 show no indication for large-angle scattering for Xe films up to 2 ML thick. The angular information agrees well with the observation that the kinetic-energy distribution of these ions does not change upon penetration of a Kr film less than 2 ML thick (Fig. 9). However, for thicker films we see evidence for elastic scattering: the energy distribution changes [Fig. 9(b)], and the angular distribution changes, as we have concluded also for Xe from the data in Fig. 8. As discussed above, the ions that change their trajectories have scattered by a rather large angle ($>10°$). This result does not seem surprising, considering the small collision energies and the large mass difference between the projectile (16 amu) and the target atoms (40, 84, and 129 amu). As is known from classical scattering calculations, the scattering angle increases with decreasing impact parameter. Since the impact parameter range is limited to less than one half of the rare-gas-rare-gas distance in the film,[35] we expect to observe scattering by large angles for thicker films, as reported in Fig. 8. As can be concluded from Fig. 9(b) and from Fig. 2 in Sack, Akbulut, and Madey,[22] the energy distribution of the scattered ions has also changed, which could be either due to a stronger attenuation of the faster ions which we consider as unlikely to explain the occurrence of the second peak, or to energy loss of fast ions which thereby become slow ions. The change is stronger for Xe than for Kr for coverages that lead to comparable O^+ attenuation (e.g., 2.5 ML of Kr and 3.3 ML of Xe). However, the energy shift is larger for Kr than for Xe, which we explain with the larger energy transfer in an O^+-Kr collision compared to O^+-Xe, due to krypton's smaller mass.

In fact, it is interesting to compare the observed energy shift with the result of a simple two-body kinematics calculation for elastic scattering between O^+ and the rare-gas atoms. We calculate the energy loss ΔE of an O^+ ion in a collision with a rare-gas atom as a function of the scattering angle θ (laboratory system);

$$\Delta E = E_0 \left[1 - \left[\frac{(m_{\text{RG}}^2 - m_{\text{O}^+}^2 \sin^2\theta)^{0.5} + m_{\text{O}^+}\cos\theta}{m_{\text{RG}} + m_{\text{O}^+}} \right]^2 \right] . \tag{8}$$

TABLE I. Results of a calculation of the kinematics of elastic scattering. See text for explanations. Collision energy is 7 eV.

θ (degrees)	ΔE (eV) for O^+-Kr	ΔE (eV) for O^+-Xe
20	0.16	0.10
30	0.35	0.22
40	0.60	0.38
50	0.90	0.57
60	1.2	0.79
70	1.6	1.0
80	1.9	1.3
90	2.2	1.5

We consider that those ions, that have lost kinetic energy [see Figs. 10(c) and 10(d)] have changed their trajectory by an angle of more than 22° (this is the solid angle of detection under 0-V sample bias). We tabulate the energy loss in Table I. From Figs. 9(b) and 2 in Sack, Akbulut, and Madey[22] we estimate the energy loss of the O^+ ions for Kr to 3 ± 0.5 eV and for Xe to 2 ± 0.5 eV. The energy losses are slightly larger than those calculated for a scattering angle of 90° which may indicate that the energy loss is not the result of one binary collision but of multiple collisions; however, the ratio of the energy loss in Kr to that in Xe is very similar to the calculated results. Note that the energy of the second peak may be shifted slightly towards lower energy due to the low-energy shoulder caused by the planar detector design (see discussion above).

So far we have only discussed the energy loss of some of the oxygen ions in the rare-gas film. Since we have demonstrated that elastic forward scattering occurs, it seems reasonable to assume that elastic backscattering should occur, too. We expect that elastic scattering by angles large enough to deflect the O^+ so that it backscatters and subsequently becomes neutralized or trapped in the solid, is one of the reasons for the attenuation of the oxygen ions in the rare-gas films.

Klein, Urbassek, and Vicanek have performed a molecular-dynamics simulation in order to simulate the elastic scattering of the O^+ ions in the rare-gas films while ignoring inelastic scattering events. As mentioned above, they assume an fcc structure for the rare-gas solid and incommensurate growth of the rare-gas films on the oxide from coverages above 1 ML. They find Kr films to have the highest attenuation cross section, which they attribute to the fact that both their backscattering and their stopping cross sections are high. There is good agreement of the simulation with the experimental data for Kr and Xe which indicates that elastic backscattering is indeed the dominant cause for attenuation of the O^+ ions in the films. The results of their simulation are published in the following paper.[11]

While Klein, Urbassek, and Vicanek[11] find good agreement of the simulation with the experimental data for Kr and Xe, the experimental data show stronger attenuation for O^+ through Ar than the simulation indicates. This suggests that Ar cannot be explained in a model that considers only elastic scattering processes and assumes an incommensurate fcc growth of the rare-gas film. It may point to the importance of another attenuation mechanism not taken into account for in the simulation, such as charge transfer.

2. *Charge transfer*

Charge transfer in ion-atom collisions can be described by

$$A^+ + B \rightarrow A' + B^+ + \Delta E \ , \tag{9}$$

where A' can be either a ground-state atom A or the atom in an excited state, and where ΔE is the energy defect. While the cross sections for resonant charge transfer (molecule A = molecule B) are relatively well understood and tabulated,[36] the nonresonant case has mainly been studied for collision energies E_c above 50 eV.[8,9]

The cross section, in the most general form, can be written as

$$\sigma_{i\rightarrow f}(E_c) = 2\pi \int_0^\infty P_{i\rightarrow f}(b, E_c) b \, db \tag{10}$$

with $P_{i\rightarrow f}$ being the probability for charge transfer, b is the impact parameter, E_c is the collision energy, and i, f is the initial and final state. Rapp and Francis developed a theoretical model for charge transfer in the nonresonant case[37]. For the nonresonant case, the cross section exhibits a maximum at that energy at which

$$\tau_c \approx \tau_{\rm ct} \tag{11}$$

with τ_c being a collision time and $\tau_{\rm ct}$ related to the energy defect ΔE by

$$\tau_{\rm ct} \Delta E \approx h \ . \tag{12}$$

The cross section decreases towards higher collision energies due to a decreasing interaction time. For collision energies below the energy at which this maximum occurs, Rapp and Francis derive the approximation

$$\sigma \cong \frac{10.8 \times h^4}{\pi} \frac{\gamma^2 v_c^4}{a_0^2 \Delta E^4} \tag{13}$$

with $\gamma = \sqrt{E_B / 13.6 eV}$, E_B ionization potential of B, v_c relative collision velocity, and a_0 Bohr radius.

Equation (13) implies that the charge-transfer cross section is higher for smaller energy defects and decreases for lower collision energies.

The collision energies that occur in our experiment are far below the energy at which the maximum in the cross section occurs (usually on the order of 1 keV).

We depict some energy levels (for infinite atomic separation) for single atoms in Fig. 12, derived from the gas phase ionization potentials of 13.6 eV for O, 15.8 eV for Ar, 14.0 eV for Kr, and 12.1 eV for Xe.[33] Shown are possible transitions involving ground-state atoms or ions, and transitions involving the excited oxygen state O*. The energy defect is smallest for Kr, 0.4 eV. It is strongly endothermic for Ar and exothermic for Xe. Therefore, in the model of Rapp and Francis, one would expect in a gas phase collision of O^+ with a rare-gas atom the largest

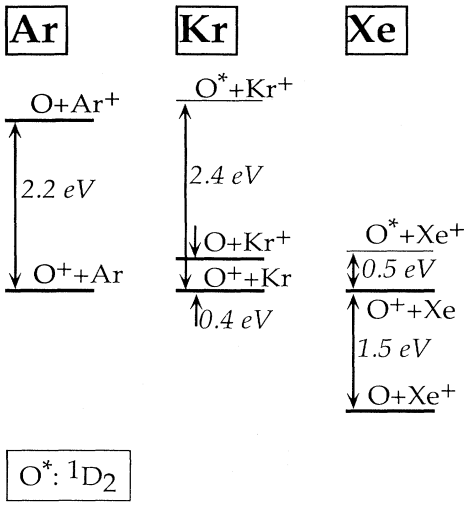

FIG. 12. Some atomic energy levels of O-Ar, O-Kr, and O-Xe. See text.

cross section for Kr. We can calculate from Eq. (13) cross sections for the charge-transfer reactions with the smallest energy defects (O^+ energy: 7 eV):

$$O^+ + Ar \rightarrow O + Ar^+, \quad \Delta E = 2.176 \text{ eV} \tag{14}$$

has a cross section of 1.8×10^{-18} cm^2.

$$O^+ + Kr \rightarrow O + Kr^+, \quad \Delta E = 0.382 \text{ eV} \tag{15}$$

has a cross section of 1.7×10^{-15} cm^2.

$$O^+ + Xe \rightarrow O(^1D_2) + Xe^+, \quad \Delta E = -0.483 \text{ eV} \tag{16}$$

has a cross section of 5.9×10^{-16} cm^2.

Hence the model by Rapp and Francis predicts a very small charge-transfer cross section for O^+-Ar.

However, one has to caution about the application of the model of Rapp and Francis: The low-energy approximation given in Eq. (13) has been developed for collision energies of >100 eV; the validity of the model at 7 eV or less is questionable. Furthermore, the model does not apply when the potential-energy surfaces involved in the charge-transfer process cross; in this case the cross sections may be higher.

Furthermore, our situation cannot be described accurately by ion-atom collisions. It has been shown that the energy levels of a rare-gas atom adsorbed on a metal surface differ significantly from those of the free atom, thereby changing the ionization potential.[35,38,39] For Ar adsorbed on Pt(111), the 5p energy level shifts up in energy towards the vacuum level by 2.9 eV. Similar effects should occur for Ar, Kr, and Xe adsorbed on the oxidized W(100) surface. However, energy-level shifts should also occur for the oxygen ion, thereby canceling most of the effect of the shifts on the energy defect for rare-gas coverages of <2 ML. In contrast to monolayer adsorbates, it seems possible that accidental resonant charge transfer may occur between O^+ and a thick rare-gas film with a band structure, because the lowest ionization energy of solid argon is 13.9 eV which is very close to that of O^+, 13.6 eV. However, we observe strong attenuation of O^+ upon passage of 1–2-ML-thick Ar films, at which thickness the band structure is not likely to be developed. Note that there is also the possibility that the rare-gas film may be excited in the vicinity in which the O^+ desorbs from the surface, due to the interaction of the primary electrons with the rare-gas film. Free excitons in solid Ar have a lifetime of $\sim 10^{-12}$ s,[40] which is longer than the time it takes for the O^+ to pass one monolayer of Ar, which is 4×10^{-14} s. The charge-transfer cross sections could be significantly affected by the presence of the excitons.

For all of the above reasons, we see little chance to predict neutralization probabilities accurately for O^+ in the rare-gas film based on the model by Rapp and Francis. The deviation of the simulation[11] from the experimental data for Ar may be caused by some form of charge transfer, although it seems difficult to understand why charge transfer should be important for O^+-Ar, which has a high endothermic energy defect.

The deviation of the simulation could also be due to a rare-gas structure different from fcc: If the Ar atoms in the first layer adsorb preferentially on top of W atoms (which could lead to a lower atom density than the bulk, as observed by TDS), and if the second layer adsorbs preferentially on top of oxygen atoms, then the transmission through the second layer could be lower than through the second layer of a regular fcc structure, and this could explain the difference between simulation and experiment.

V. CONCLUSIONS

With our experimental approach, we have demonstrated that cross sections for interaction of 7-eV O^+ with rare gases are sufficiently low that some oxygen ions can penetrate several layers of a rare-gas solid; secondary ions are detected which originate several layers below the surface. We have found indications for elastic scattering of the ions in the film. Since the experimental results for Kr and Xe agree well with the MD simulation by Klein, Urbassek, and Vicanek,[11] we attribute the attenuation of O^+ in Kr and Xe primarily to elastic backscattering. Surprisingly, the attenuation is very strong for argon and also stronger than predicted by the MD simulation so that we suggest that either charge transfer between O^+ and the Ar film (which has not been taken into account in the simulation) could be an additional cause for the O^+ attenuation, or, more likely, an Ar structure different from fcc. We suggest that the deviation of the attenuation from a strictly exponential behavior is an indication that the fcc structure of rare-gas solids allows some O^+ to channel through the first two layers without strong attenuation. We conclude that for the question of depth of origin of secondary ions from surfaces it is important to consider the structure of the surface as well as the interaction potential of the ion with the atoms in the surface layer. We should caution that compound surfaces are usually more densely packed than rare-gas solids, so that ions desorbing from such surfaces may not penetrate

as far as it has been observed here. This is the first in a series of studies concerning the question of depth or origin of secondary ions through rare gas layers. Future investigations will involve other ions (both positive and negative) through rare-gas layers as well as molecular overlayers, such as water and ammonia.

ACKNOWLEDGMENTS

We acknowledge helpful discussions and correspondence with H. Urbassek, M. Vicanek, R. A. Baragiola, and R. E. Johnson; we also thank P. Klein, H. M. Urbassek, and M. Vicanek for a pleasant collaboration.

*Permanent address: Department of Physics, Stevens Institute of Technology, Hoboken, NJ 07030.

[1]J. W. Burnett, J. P. Biersack, D. M. Gruen, B. Jørgensen, A. R. Kraus, M. J. Pellin, E. L. Schweitzer, J. T. Yates, Jr., and C. E. Young, J. Vac. Sci. Technol. A **6**, 2064 (1988).

[2]P. Sigmund, A. Oliva, and G. Falcone, Nucl. Instrum. Methods **194**, 541 (1982).

[3]M. Vicanek, J. J. J. Rodriguez, and P. Sigmund, Nucl. Instrum. Methods Phys. Res. Sect. B **36**, 124 (1989).

[4]P. Sigmund *et al.*, Nucl. Instrum. Methods Phys. Res. Sect. B **36**, 110 (1989).

[5]M. F. Dumke, T. A. Tombrello, R. A. Weller, R. M. Housley, and E. H. Cirlin, Surf. Sci. **124**, 407 (1983).

[6]H. Allali, B. Cabaud, G. Fuchs, A. Hoareau, B. Nsouli, J.-P. Thomas, M. Treilleux, and J.-S. Danel, Nucl. Instrum. Methods Phys. Res. Sect. B **84**, 303 (1994).

[7]U. Diebold and T. E. Madey, Phys. Rev. Lett. **72**, 1116 (1994).

[8]J. B. Hasted, *Physics of Atomic Collisions* (American Elsevier, New York, 1972).

[9]H. Massey and H. Gilbody, *Electronic and Ionic Impact Phenomena* (Clarendon, Oxford, 1974).

[10]N. J. Sack, M. Akbulut, and T. E. Madey, Nucl. Instrum. Methods Phys. Res. Sect. B **90**, 451 (1994).

[11]P. Klein, H. Urbassek, and M. Vicanek, following paper, Phys. Rev. B **51**, 4597 (1995).

[12]D. A. King. T. E. Madey, and J. T. Yates, Jr., J. Chem. Phys. **55**, 3236 (1971).

[13]D. A. King, T. E. Madey, and J. T. Yates, Jr., J. Chem. Phys. **55**, 3247 (1971).

[14]T. E. Madey and J. T. Yates, Jr., Surf. Sci. **11**, 327 (1968).

[15]T. E. Madey, J. J. Czyzewski, and J. T. Yates, Jr., Surf. Sci. **49**, 465 (1975).

[16]S. Prigge, H. Niehus, and E. Bauer, Surf. Sci. **75**, 635 (1978).

[17]M. L. Knotek and P. J. Feibelman, Phys. Rev. Lett. **40**, 964 (1978).

[18]R. D. Ramsier and J. T. Yates, Jr., Surf. Sci. Rep. **12**, 243 (1991).

[19]R. Opila and R. Gomer, Surf. Sci. **112**, 1 (1981).

[20]N. J. Sack, M. Akbulut, and T. E. Madey (unpublished).

[21]H. Schlichting and D. Menzel, Surf. Sci. **272**, 27 (1992).

[22]N. J. Sack, M. Akbulut, and T. E. Madey, Phys. Rev. Lett. **73**, 794 (1994).

[23]L. J. Kieffer, At. Data **1**, 19 (1969).

[24]J. E. Houston and T. E. Madey, Phys. Rev. B **26**, 554 (1982).

[25]Q. J. Zhang and R. Gomer, Surf. Sci. **109**, 567 (1981).

[26]Q. J. Zhang, R. Gomer, and S. R. Bowman, Surf. Sci. **129**, 535 (1983).

[27]B. Krahl-Urban and H. Niehus, Surf. Sci. **88**, L19 (1979).

[28]T. E. Madey, Surf. Sci. **94**, 483 (1980).

[29]M. F. Guest, A. Ding, J. Karlau, J. Weise, and I. H. Hillier, Mol. Phys. **38**, 1427 (1979).

[30]R. C. Weast, *CRC Handbook of Chemistry and Physics* (CRC, Boca Raton, FL, 1988).

[31]P. Dai, Z. Wu, H. Taub, and S. N. Ehrlich (unpublished).

[32]J. M. Layet, M. Bienfait, C. Ramseyer, P. N. M. Hoang, C. Girardet, and G. Coddens, Phys. Rev. B **48**, 9045 (1993).

[33]C. Kittel, *Introduction to Solid State Physics* (Wiley, New York, 1986).

[34]R. E. Johnson, *Energetic Charged-Particle Interactions with Atmospheres and Surfaces* (Springer-Verlag, Berlin, 1990).

[35]N. Schwentner, E.-E. Koch, and J. Jortner, *Electronic Excitations in Condensed Rare Gases* (Springer-Verlag, Berlin, 1985).

[36]S. Sakabe and Y. Izawa, At. Data Nucl. Data Tables **49**, 257 (1991).

[37]D. Rapp and W. E. Francis, J. Chem. Phys. **37**, 2631 (1962).

[38]G. Schönhense, A. Eyers, and U. Heinzmann, Phys. Rev. Lett. **56**, 512 (1986).

[39]D. Menzel, Appl. Phys. A **51**, 163 (1990).

[40]E. Hudel, E. Steinacker, and P. Feulner, Phys. Rev. B **44**, 8972 (1991).